Published in final edited form as:

J Mater Chem B. 2019 November 07; 7(41): 6449–6457. doi:10.1039/c9tb01918a.

Hydroxyapatite-binding micelles for the detection of vascular calcification in atherosclerosis

Deborah D. Chin[a], **Jonathan Wang**[a], **Margot Mel de Fontenay**[a], **Anastasia Plotkin**[b], **Gregory A. Magee**[b], **Eun Ji Chung**[a,b,c,d,e,f]

[a]Department of Biomedical Engineering, University of Southern California, Los Angeles, CA, USA

[b]Department of Surgery, Division of Vascular Surgery and Endovascular Therapy, Keck School of Medicine, University of Southern California, Los Angeles, CA, USA

[c]Eli and Edythe Broad Center for Regenerative Medicine and Stem Cell Research, Keck School of Medicine, University of Southern California, Los Angeles, CA, USA

[d]Norris Comprehensive Cancer Center, Keck School of Medicine, University of Southern California, Los Angeles, CA, USA

[e]Department of Chemical Engineering and Materials Science, University of Southern California, Los Angeles, CA, USA

[f]Department of Medicine, Division of Nephrology and Hypertension, Keck School of Medicine, University of Southern California, Los Angeles, CA, USA

Abstract

Atherosclerosis is a chronic disease characterized by the formation of calcified, arterial plaques. Microcalcifications (5 μm to 100 μm), mainly composed of hydroxyapatite (HA, $Ca_5(PO_4)_3(OH)$), develop in the fibrous caps of atherosclerotic plaques and can trigger plaque rupture due to the loss of compliance and elasticity. Ultimately, plaque rupture can cause arterial occlusion and embolization and result in ischemic events such as strokes and myocardial infarctions. Unfortunately, current imaging technologies used to detect calcifications are limited by low signal-to-noise ratio or use invasive procedures that pose risk of arterial dissection. To mitigate these drawbacks, in our study, we developed a novel, fluorescently-labeled peptide amphiphile micelle (PAM) that uses a 12 amino acid HA-binding peptide (HABP) [SVSVGMKPSPRP] to target and detect atherosclerotic calcification (HA PAM). Our results show HA PAMs can successfully target HA microcrystals with a strong binding affinity (K_D = 6.26 ± 1.2 μM) *in vitro*. In addition, HA PAMs detected HA mineralization (HA PAM vs. non-targeting micelle, $p \leq 0.001$; HA PAM vs. scrambled HABP PAM, $p \leq 0.01$) formed by calcifying mouse aortic vascular smooth muscle cells (MOVAS). Moreover, HA PAMs successfully detected calcifications in atherosclerotic mouse models as well as in patient-derived arteries. Our studies show that HA PAMs show promise as calcium-targeting nanoparticles for the detection of calcifications in atherosclerosis.

Electronic Supplementary Information (ESI) available]. See DOI: 10.1039/x0xx00000x

Conflicts of interest

There are no conflicts of interest to declare.

Introduction

Vascular calcification found in patients with atherosclerosis is correlated with thrombosis, myocardial infarction, and cardiovascular morbidity.[1–3] Specifically, calcification is initiated by vascular smooth muscle cells (VSMCs) found within the arterial wall that obtain an osteoblast-like phenotype during atherosclerosis and release hydroxyapatite (HA).[4, 5] Upon HA aggregation, the outer, fibrous cap of plaques can become embedded with microcalcification nodules ranging from 5 μm to 65 μm that cause mechanical instability and mismatch between the calcification nodules and the surrounding tissue, and lead to plaque rupture.[5, 6]

Computer modelling and analysis of calcified, human atherosclerotic plaques have further corroborated that microcalcifications within the fibrous cap significantly contribute to plaque destabilization.[7] As the vessel undergoes tensile stress, cavitations are formed between calcifications that propagate fracture and plaque rupture. Hence, detection of calcifications within atherosclerotic plaques may have the potential to determine rupture-prone plaques before the occurrence of acute ischemic events.

Current imaging modalities to detect calcification include computed tomography (CT), intravascular ultrasound (IVUS), and optical coherence tomography (OCT). Although the gold standard for detecting arterial calcification is CT, CT requires exposure to ionizing radiation that can cause mutations or apoptosis in surrounding cells.[8] In addition, CT scans using iodinated contrast agents suffer drawbacks such as nonspecific biodistribution, rapid renal clearance, and renal toxicity[9], calling for the need of targeted contrast agents.[10] External ultrasonography can detect arterial calcification, but there is no widely accepted method to quantify the degree of calcification and is not easily applicable to coronary arteries.[11] IVUS and OCT are excellent tools to assess vessel stenosis, but are invasive procedures that are limited by a low signal-to-noise ratio and minimal calcium penetration.[12–14] Thus, the development of a safe and noninvasive contrast agent that selectively binds to HA would aid in the identification of plaque-rupturing calcifications.

Recently, nanoparticles have demonstrated potential as diagnostic tools with multimodal functionality and versatile physiochemical properties.[10, 15–20] By manipulating size, surface charge, and shape, nanoparticles can be specially designed to penetrate tissue and target diseased sites with minimal toxicity.[16, 21, 22] In our study, we developed self-assembling, peptide amphiphile micelle (PAM) nanoparticles that utilize HA-binding peptides (HABP) as targeting ligands to bind to HA for the identification of microcalcifications found in plaques (Scheme 1). Specifically, we integrated a 12 amino acid peptide sequence [SVSVGMKPSPRP] (HABP) previously identified via phage display for highly specific binding to HA.[23] In addition, we incorporated fluorescein isothiocyanate (FITC) or the near-infrared (NIR) fluorescent dye, Cyanine 7 (Cy7), into our micelle platform to detect and image calcifications. Together, we show that this novel HA-targeting PAM (HA PAM) has potential to selectively bind and detect calcification using *in vitro* models of calcified VSMC, the apolipoprotein E-deficient (ApoE −/−) murine model of atherosclerosis, as well as on patient-derived, diseased arteries.

Materials and methods

HA-binding peptide synthesis

HA PAMs were synthesized as previously described.[15, 24] Briefly, HA-binding peptides (HABP) of sequence [CSVSVGMKPSPRP][23] and scrambled HABP [CVRVSSPPMPGSK] were synthesized using standard Fmoc-mediated solid phase peptide synthesis on an automatic PS3 benchtop peptide synthesizer (Protein Technologies, Tucson, AZ, USA). The cysteine residue at the N-terminus was used for thioether linkage. The peptides were then N-capped with an acetyl group and cleaved from the rink amide resin using 94:2.5:2.5:1 volume ratios of trifluoroacetic acid:1,2 ethanedithiol:H_2O:triisopropylsilane. Cleaved peptides were precipitated and washed several times with ice cold diethyl ether, subsequently dissolved in Milli-Q water, and lyophilized. Lyophilized peptides were stored at −20°C until purification using reverse-phase high performance liquid chromatography (HPLC, Fig. S1, Phenomenex, Torrance, CA, USA; Shimadzu, Kyoto, Japan). Crude peptides were purified using a C8 column (Phenomenex, Torrance, CA, USA) at 55°C using 0.1% formic acid in acetonitrile/water mixture. Purified samples were characterized and verified using Matrix Assisted Laser Desorption/Ionization-Time of Flight (MALDI-TOF) mass spectral analysis (Fig. S2, Bruker, Billerica, MA, USA). Pure peptides were conjugated to create amphiphiles via a thioether linkage to 1,2 distearoyl-*sn*-glycero-3-phosphoethanolamine-*N*-[maleimide(polyethylene glycol)-2000], or DSPE-PEG(2000)-maleimide (Nanocs, New York, NY, USA) by adding a 10% molar excess of the peptide to lipid in water. The pH of the mixture was adjusted to 7 and the solution was left to react at room temperature for 24 hours with constant agitation until further purification using a C4 column (Phenomenex, Torrance, CA, USA) and verified using MALDI-TOF.

Micelle synthesis

Multimodal micelles were synthesized by mixing HABP amphiphiles or scrambled HABP amphiphiles with DSPE-PEG(2000)-FITC (excitation/emission wavelength: 490/525 nm, PEGworks, Durham, NC, USA) or DSPE-PEG(2000)-Cy7 (excitation/emission wavelength: 750/773 nm, Lumiprobe, Hunt Valley, MD, USA) at a 90:10 mole ratio in a methanol solution.[25,26] Methanol was evaporated using nitrogen and the resulting lipid film was dried overnight under vacuum. The lipid film was then hydrated in phosphate buffered saline (PBS) or Milli-Q water, incubated at 80°C for 30 minutes to allow self-assembly and cooled to room temperature. Non-targeting micelles (NT micelles) were assembled using DSPE-PEG(2000)-methoxy (Avanti, Alabaster, AL, USA) and fluorophore amphiphile at a 90:10 mole ratio.

Dynamic light scattering (DLS)

Micelle diameter and zeta potential was measured using DLS at a concentration of 100 μM in Milli-Q water (N≥3). DLS measurements were determined at 90° and 637 nm using a Wyatt DynaPro Mobius (Wyatt, Santa Barbara, CA, USA).

Transmission electron microscopy (TEM)

HA PAMs in Milli-Q water (100 μM) were placed onto a 400 mesh carbon TEM grid (Ted Pella, Redding, CA, USA) for 2 minutes. Excess solution was removed and the TEM grid was briefly washed with Milli-Q water before negatively staining the micelles using 2 wt% uranyl acetate solution (Polysciences, Warrington, PA, USA). The stain was removed, and the grid washed once more with water. Samples were dried and imaged on a JEOL 2100F (JEOL, Tokyo, Japan, N=3).

Cell culture and *in vitro* cellular calcification

Mouse aortic vascular smooth muscle (MOVAS) cells (ATCC, Manassas, VA, USA) were cultured in Dulbecco's Modified Eagle Medium (Gibco, Waltham, MA, USA) with 10 vol% fetal bovine serum and 0.2 mg/ml G-418 (Gibco, Waltham, MA, USA). Only cells of passage 3–5 were used for experiments. Cells were grown to confluence when introduced to osteogenic media containing 10 mM β-glycerophosphate, 50 μg/ml L-ascorbic acid, and 0.1 μM dexamethasone (Sigma-Aldrich, St Louis, MO, USA).[27, 28] Cells were cultured in osteogenic media for 21 days, and media was changed every 2–3 days.

Scanning electron microscopy (SEM) and energy dispersive spectroscopy (EDAX)

HA microcrystals (Sigma-Aldrich, St Louis, MO, USA) of 10 μm diameter were imaged and analyzed for calcium:phosphate ratio using SEM and EDAX. HA minerals were attached to a sample holder, sputter coated with palladium, and then imaged using JEOL 7001F (JEOL, Tokyo, Japan, N=3). EDAX was used to analyze calcium and phosphate elemental composition of HA minerals.

HA PAM binding on HA microcrystals and binding isotherms

FITC-labeled HA PAMs and NT micelles (5 and 10 μM) were synthesized and incubated with 5 mg of HA microcrystals (Sigma-Aldrich, St Louis, MO, USA) at room temperature in PBS for 1 hour with constant agitation to facilitate binding. The amount of micelles bound was determined by measuring the amount of unbound micelles through fluorescence readings and comparing with a standard curve (N=6). The dissociation constant, K_D, of HA PAM was determined by fitting HA PAM binding at different micelle concentrations (0.50, 0.75, 1, 1.5, 2, 3, 4, 5, 10 μM) to a single site-specific binding model,

$$\Delta m = \left(B_{max} * C\right)/\left(K_D + C\right),$$

where Δm is the amount of adsorbed PAM, C is the concentration of PAM in solution, B_{max} is the maximum adsorption, and K_D is the dissociation constant (GraphPad Prism 7, San Diego, CA, USA, N=3).[29] To further verify HA PAM binding to HA microcrystals, HA PAM- and NT micelle-bound HA microcrystals were imaged under a fluorescence microscope (Leica DMi8, Leica, Wetzlar, Germany, N=6).

HA competition assay

HA microcrystals (Sigma-Aldrich, St Louis, MO, USA) were incubated with HABPs or scrambled HABPs for 1 hour at 1 mM concentrations. HABPs or scrambled HABPs were

removed and HA microcrystals were then incubated with FITC-labeled HA PAMs (5 μM) and the amount of HA PAMs bound was measured indirectly through fluorescence readings using a microplate reader (excitation/emission: 490/525, Varioskan LUX, Thermo Fisher Scientific, Waltham, MA, USA, N=6).

Cell calcium mineralization assay

After culturing in osteogenic media for 7, 14, and 21 days, MOVAS cells were fixed in 4% paraformaldehyde and stained with 2% Alizarin red S (ARS) solution (pH 4.2, ScienCell, Carlsbad, CA, USA) for 30 minutes at room temperature, following the manufacturer's protocol. Brightfield images were taken of calcium-stained cells using a Leica DMi8 (Leica, Wetzlar, Germany). Cellular calcification was quantified via ARS dye extraction by incubating the cells with 10% acetic acid for 30 minutes with constant agitation.[30] Cells and calcium deposits were then collected, heated to 85°C for 10 minutes, and centrifuged at 20,000 $x\,g$ for 15 minutes. The supernatant containing the extracted ARS dye was collected and absorbance was measured at 405 nm using a microplate reader (Varioskan LUX, Thermo Fisher Scientific, Waltham, MA, USA, N=6).

Alkaline phosphatase assay

Cellular calcification was also determined by measuring alkaline phosphatase (ALP) enzyme activity. Briefly, calcifying cells were lysed using 0.2% Triton x-100, 3 mM sodium bicarbonate, and 150 mM sodium chloride (Sigma-Aldrich, St Louis, MO, USA). P-nitrophenyl phosphate (10 mM) was added to lysed cells and incubated at 37°C for 10 minutes.[31] Phosphatase activity was stopped with 0.1 M sodium hydroxide. Cells and substrate solution were collected and centrifuged at 16,000 $x\,g$ for 10 minutes. Absorbance of the supernatant was measured at 405 nm using a microplate reader (N=6). Enzyme activity was calculated by comparing to a standard curve and using the equation:

$$ALP\ activity\ (U/ml) = A/V/T,$$

where A is the amount of p-nitrophenol produced, V is the volume, and T is the reaction time.

In vitro biocompatibility

MOVAS cells were incubated with HA PAMs, HA scrambled PAMs (HA scram PAMs), NT micelles, HABPs, scrambled HABPs (1, 10, 100 μM), or PBS control for 48 hours before biocompatibility was assessed using a Live/Dead cell viability assay and MTS (3-(4,5-dimethylthiazol-2-yl)-5-(3-carboxymethoxyphenyl)-2-(4-sulfophenyl)-2H-tetrazolium) cell proliferation assay (Biovision, Milpitas, CA, USA). For the Live/Dead cell viability assay, MOVAS cells were stained in live and dead cell staining dyes for 15 minutes at 37°C and subsequently imaged on a fluorescence microscope (Leica DMi8, Leica, Wetzlar, Germany, N=6). For the MTS assay, after 48 hours of treatment, MOVAS cells were incubated with MTS reagent for 1 hour at 37°C. Absorbance of the MTS reagent was measured using a plate reader at 490 nm (N=6). Cell viability was calculated by comparing with untreated cells.

In vitro cellular calcification binding assays

MOVAS cells were calcified for 21 days before HA PAM, HA scram PAM, and NT micelle binding was assessed. Micelle binding was determined indirectly by measuring the amount of unbound micelles. FITC-labeled HA PAMs, HA scram PAMs, or NT micelles (10 μM) were incubated with calcified MOVAS cells at 37°C for 1 hour. Micelles were then removed and measured for FITC fluorescence at 490/525 nm using a plate reader (Varioskan LUX, Thermo Fisher Scientific, Waltham, MA, USA, N=8). In addition, micelle binding to calcifications was confirmed through fluorescence microscopy. After removing the micelles, cells grown in osteogenic or growth media for 21 days were fixed in 4% paraformaldehyde, stained for calcification using 0.00005% ARS, and imaged on a fluorescence microscope (Leica DMi8, Leica, Wetzlar, Germany). DAPI was used to stain nuclei.

HA PAM binding *in vivo* on ApoE −/− mice

Cy7-containing HA PAMs were used to test binding to calcification in atherosclerotic plaque *in vivo* using ApoE −/− mice. Male and female, nine-month-old ApoE −/− mice (Jackson Laboratory, Bar Harbor, ME, USA) were fed a Western diet for 6 weeks (Envigo, Huntingdon, UK). Mice were injected with 100 μL of HA PAMs, HA scram PAMs, NT micelles (N=4, 1000 μM), Osteosense, or PBS via tail vein injection (N=3). Osteosense is a commercially available NIR bisphosphonate-based calcium tracer used for *in vivo* bone and calcification imaging in atherosclerotic animal models.[32–35] It has excitation and emission wavelengths at 745 nm and 800 nm (Osteosense 750, PerkinElmer, Waltham, MA, USA). Osteosense was used to serve as a comparison for HA PAM targeting efficacy.

Mice were then euthanized 24 hours after injection and the aorta and organs harvested, including the heart, lungs, liver, kidneys, spleen, stomach, intestine, and bladder. Ex vivo imaging was conducted using Ami HTX (Spectral Instruments Imaging, Tucson, AZ, USA) and fluorescence was analyzed to determine the biodistribution of particles. Harvested tissues were embedded in Optimal Cutting Temperature (OCT) compound, flash frozen in 2-methylbutane and liquid nitrogen, and sectioned using a cryostat (10 μm thickness, Leica CM3050S, Leica, Wetzlar, Germany). Tissue sections were then stained with hematoxylin and eosin (H&E), ARS, or DAPI, mounted, and imaged using a fluorescence microscope (Leica DMi8). All mice experiments were approved by and performed in compliance with the University of Southern California (USC) Institutional Animal Care and Use Committee (IACUC).

HA PAM binding on patient-derived arteries

Tibial arteries were obtained from discarded tissue from patients with peripheral vascular disease (N=3, 47- and 52-year-old males with severely calcified tibial arteries). The collection of discarded tissue for human subjects research was approved by the USC Institutional Review Board (HS-18–00638, BUA-18–00031) and tissue was obtained after informed patient consent. Arteries were washed several times in Hank's Balanced Salt Solution (HBSS). The tissues were then incubated with FITC-labeled HA PAMs or NT micelles for 1 hour at 37°C. Afterwards, the tissue was cryoprotected in 15% sucrose, embedded in OCT compound, and flash frozen. Tissues were sectioned using a cryostat (10 μm thicknesses, Leica CM3050S) and stained with 0.00005% or 2% ARS, dehydrated, and

mounted onto slides. Sections were also stained with H&E and imaged with a brightfield and fluorescence microscope (Leica DMi8).

Statistical analysis

Quantification data are given as mean ± standard deviation. All statistical analyses were performed using GraphPad Prism 7 (San Diego, CA, USA). A student's t-test or analysis of variance (ANOVA) was used to determine statistical significance and $p \leq 0.05$ was considered to be significant.

Results and discussion

Synthesis and characterization of HA PAMs

Roy et al. first reported that the hydroxyapatite-binding peptide (HABP) [SVSVGMKPSPRP] selectively binds to HA.[23] As HA is the predominant calcium mineral found in atherosclerotic calcifications, we incorporated HABPs into our micelle system to target calcifications found in atherosclerotic plaques (Scheme 1).[3]

Micelles were fabricated at 5–100 μM which is above the critical micelle concentration for DSPE-PEG(2000)-based micelles.[15] TEM micrographs showed a homogenous population of spherical micelles and DLS confirmed micelles had a small polydispersity index (PDI) of 0.30 ± 0.04 and 0.13 ± 0.02 for HA PAMs and NT micelles, respectively (Fig. 1, Table 1). The two particles were similar in size with radii of 8.0 ± 1.5 nm and 6.6 ± 0.3 nm for HA PAMs and NT micelles, respectively. Zeta potential of HA PAMs (−2.7 ± 2.2 mV) and NT micelles (−0.9 ± 1.1 mV) were found to be slightly negative, which can be attributed to the maleimide group and phosphate group in the DSPE lipid tail. HA scram PAMs had radii of 8.9 ± 1.1 nm and zeta potential of −0.1 ± 0.6 mV (Table S1). Nonetheless, all particles fell within physiologically neutral charge ranges for enhanced circulation times *in vivo*.[36, 37]

HA PAM binding on HA microcrystals *in vitro*

In order to examine the potential of HA PAMs to target HA calcifications, FITC-labeled HA PAMs (5 μM, green) were incubated with HA microcrystals for 1 hour and examined by fluorescence microscopy (Fig. 2A). Unlike NT micelles which showed minimal binding, HA PAMs bound to HA microcrystals and fluorescence signal from HA PAMs could be detected on the microcrystals, confirming specificity of the nanoparticles to HA.

To quantify micelle binding, we incubated HA PAMs with HA microcrystals at 5 and 10 μM (Fig. 2B). At 5 μM, 39 ± 1.8% of HA PAM showed binding onto HA microcrystals compared to 23 ± 1.0% for NT micelles ($p \leq 0.0001$, N=6). At 10 μM, there was an increased percentage of both HA PAMs and NT micelles bound to HA. Nonetheless, HA PAMs had 83 ± 0.8% of micelles bound compared to 75 ± 2.4% for NT micelles, which was found to be statistically significant ($p \leq 0.0001$, N=6). To further verify the binding specificity of our HA PAMs to HA, HA microcrystals were preincubated with either HABPs or scrambled HABPs (scram peptide) for 1 hour before adding HA PAMs in a competition assay. HA PAMs had a higher percentage of particles bound to HA microcrystals preincubated with scrambled HABPs when compared to microcrystals preincubated with HABPs (scram peptide: 30.5

± 4.2% vs HABP: 16.3 ± 3.6%, p≤0.0001, N=6, Fig. 2C), demonstrating the specificity of HABP as a binding ligand for HA and the effectiveness of HA PAMs.

Binding affinity of HA PAMs was evaluated via an adsorption isotherm with different concentrations of PAMs (0.50, 0.75, 1, 1.5, 2, 3, 4, 5, 10 μM) incubated with 5 mg of HA microcrystals (N=3). The K_D was determined by fitting the total amount of PAM adsorption onto HA into a single site-specific binding model, as previously demonstrated by Tang et al.[29] HA PAM possessed a K_D of 6.26 ± 1.21 μM (Fig. 2D). Notably, Weiger et al. previously reported that free HABP has a weaker binding affinity with a K_D of 14.1 ± 3.8 μM.[38] Incorporating multiple HABPs into our multivalent micelle nanoparticle may have increased the binding affinity to HA and lowered the K_D of HA PAMs as opposed to the free peptide.[29] In addition, HA PAMs have enhanced or similar binding affinity compared to other common HA-binding motifs reported in the literature. For example, alendronate bisphosphonate has a K_D of 1 mM, while acidic oligopeptides consisting of repeated Asp or Glu have a K_D of 2.5 to 12.1 μM and 2.4 to 13.1 μM, respectively, depending on the number of repeated amino acids.[39, 40] Overall, HA PAMs demonstrated specific binding to HA microcrystals similar in size to HA microcalcifications in atherosclerotic plaque.[7,41]

In vitro biocompatibility of HA PAMs

To evaluate biocompatibility of HA PAMs, MOVAS cells were treated with HA PAMs, HA scram PAMs, NT micelles, HABPs, or HA scram peptides at 1, 10, 100 μM. After 48 hours of incubation, a Live/Dead assay confirmed that all groups had minimal toxicity and was comparable to PBS-treated cells across all concentrations via fluorescence images (Fig. 3A). Furthermore, an MTS cell proliferation assay demonstrated no significant reduction in cell viability on peptide- and micelle-treated cells when normalized to PBS-treated controls, and cell viability remained above 90% across all concentrations (Fig. 3B). Consistent with other PAMs reported in the literature, HA PAMs show little cytotoxicity and are biocompatible materials, demonstrating their potential to be used as calcium-targeting agents.[15,18, 24, 42,43]

In vitro binding of micelles on calcified MOVAS

Upon confirming biocompatibility of HA PAMs, binding was also tested *in vitro* using calcified MOVAS cells. MOVAS cells were cultured in growth or osteogenic media for 7, 14 and 21 days, after which calcification was measured using an ARS dye extraction method.[30] By 14 and 21 days of culture in osteogenic media, significant calcification was detected (Fig. S3A, S3D). Moreover, an alkaline phosphatase (ALP) assay confirmed calcified MOVAS cells exhibited a 2.3-fold increase in ALP activity compared to nonosteogenic cells on day 21 (Fig. S3B).[3,44–47] After confirming calcification, HA PAMs, HA scram PAMs, or NT micelles were incubated for 1 hour with MOVAS cells calcified for 21 days. While NT micelles (1.6 ± 0.3%, p≤0.001 vs HA PAMs) and HA scram PAMs (5.3 ± 0.6%, p≤0.01 vs HA PAMs) showed a background level of binding, there was a significant increase in HA binding for HA PAMs (13.4 ± 5.7%, Fig. 4A, N=8).

In addition, to confirm HA PAMs were specific to calcified MOVAS cells, HA PAMs were incubated with MOVAS cells also cultured in regular growth media (Fig. 4B). HA PAMs exhibited statistically significant binding to calcified MOVAS cells (12.7 ± 5.7%) compared

to nonosteogenic cells (6.1 ± 1.1%, p≤0.01, N=8). Upon fluorescence microscopy, HA PAMs were found to colocalize to regions of calcification as confirmed by ARS staining (Fig. 4C, yellow), whereas NT micelles and HA scram PAMs showed minimal signal and calcium binding. In sum, our *in vitro* binding studies show HA PAMs bind to HA calcifications to a greater extent compared to NT micelles and HA scram PAMs.

In vivo HA PAM biocompatibility and targeting in atherosclerotic mice

To assess targeting *in vivo*, nine-month-old, male and female ApoE −/− mice fed a Western diet for 6 weeks (Fig. S5) were intravenously injected via tail vein with 100 μL of Cy7-containing HA PAMs, HA scram PAMs, or NT micelles (1 mM). Osteosense and PBS were also injected and used as controls. After 24 hours post-administration, aortas were harvested from the mice and *ex vivo* imaging conducted (Fig. 5A). Aortas from HA PAM-treated mice exhibited elevated fluorescence signal intensity compared to HA scram PAMs, NT micelles, and Osteosense. Of note, given that vascular calcification is prevalent in brachiocephalic arteries of ApoE−/− mice, elevated fluorescence signal in the brachiocephalic artery of HA PAM-treated mice can be correlated with calcification targeting.[48] As such, brachiocephalic arteries from each group were further sectioned and stained with ARS to confirm the presence of calcifications and micelles (Fig. 5B). While no signal was observed from NT micelle- or PBS-treated groups, HA PAMs colocalized with regions of calcification as visualized by ARS staining. Pearson's R correlation coefficient showed HA PAM had strong colocalization (0.76 ± 0.1) with ARS (Fig. 5C) compared to Osteosense which had a Pearson correlation coefficient value of 0.42 ± 0.15 (p≤0.05).

To assess biocompatibility *in vivo*, the heart, lungs, liver, spleen, intestine, and kidneys were harvested, flash frozen, and sections stained with H&E (Fig. 6). The morphology of all organs including the liver and kidneys where nanoparticles were also uptaken (Fig. S6) did not show any signs of necrosis and were found to be similar to PBS-treated controls, confirming safety of HA PAMs for *in vivo* applications.[18, 49]

Ex vivo assessment of HA PAM binding on calcified human arteries

Given that HA PAMs showed significant binding to calcified cells and mouse arteries, we tested whether HA PAMs had potential to detect calcification in patient-derived, diseased arteries. Severely calcified tibial arteries exhibiting gross bulk calcifications were collected from tissue discarded following vascular surgery. The arteries were incubated with HA PAMs or NT micelles for 1 hour, before embedding in OCT and processing for histological analysis (N=3).

Unlike NT PAMs which showed minimal binding, HA PAMs bound to calcifications of a variety of sizes (Fig. 7A). Notably, HA PAMs penetrated the arterial walls and were able to diffuse throughout the bulk calcium nodules (Fig. 7A, yellow arrow). HA PAMs (0.55 ± 0.09) showed a statistically significant increase in colocalization with calcium regions (Fig. 7B) compared to NT micelles (0.24 ± 0.04, p≤0.01). In addition to bulk calcification, HA PAMs showed the ability to bind to microcalcifications that were smaller than 50 μm (white arrow) (Fig. 7A). This suggests that HA PAMs have the potential to detect a wide range of calcifications in atherosclerosis, including those that lead to plaque instability. In

sum, our studies provide proof-of-concept data regarding the utility of HA PAMs as a novel tool in the detection and diagnosis of atherosclerotic calcification.

Conclusion

In this study, we developed a novel, peptide-based micelle that shows promise as a calcium-targeting tool for atherosclerosis. HA PAMs showed significant and specific binding to HA minerals and calcified mouse vascular smooth muscle cells *in vitro*. Moreover, HA PAMs were able to detect calcified regions of plaque in ApoE −/− mice as well as in patient-derived, calcified arteries. Future studies will test the promise of HA PAMs *in vivo* as a theranostic platform by incorporating therapeutic moieties to mitigate calcium formation and incorporate clinically-relevant imaging capabilities.

Supplementary Material

Refer to Web version on PubMed Central for supplementary material.

Acknowledgements

The authors would like to acknowledge the financial support from the Women in Science and Engineering program at USC, American Heart Association Predoctoral Fellowship (19PRE34380998) awarded to DDC, and Gabilan Assistant Professorship, L. K. Whittier Foundation, the National Heart, Lung, and Blood Institute (NHLBI, R00HL124279), and NIH New Innovator Award (DP2-DK121328) awarded to EJC. TEM images were taken with the aid of USC Center of Excellence in Nano Imaging. Lastly, we thank our patients for generously granting us permission to use their discarded tissue for this study.

References

1. Paloian NJ and Giachelli CM, Am J Physiol Renal Physiol, 2014, 307, F891–900. [PubMed: 25143458]
2. Chen NX and Moe SM, Curr Diab Rep, 2003, 3, 28–32. [PubMed: 12643143]
3. Demer LL and Tintut Y, Circulation, 2008, 117, 2938–2948. [PubMed: 18519861]
4. Iyemere VP, Proudfoot D, Weissberg PL and Shanahan CM, J Intern Med, 2006, 260, 192–210. [PubMed: 16918817]
5. New SE and Aikawa E, Arterioscler Thromb Vasc Biol, 2013, 33, 1753–1758. [PubMed: 23766262]
6. Anderson HC, Curr Rheumatol Rep, 2003, 5, 222–226. [PubMed: 12744815]
7. Kelly-Arnold A, Maldonado N, Laudier D, Aikawa E, Cardoso L and Weinbaum S, Proc Natl Acad Sci U S A, 2013, 110, 10741–10746. [PubMed: 23733926]
8. Disthabanchong S, Vipattawat K, Phakdeekitcharoen B, Kitiyakara C and Sumethkul V, Int Urol Nephrol, 2018, 50, 355–364. [PubMed: 29236239]
9. Lusic H and Grinstaff MW, Chem Rev, 2013, 113, 1641–1666. [PubMed: 23210836]
10. Li F, Li C, Liu J, Liu X, Zhao L, Bai T, Yuan Q, Kong X, Han Y, Shi Z and Feng S, Nanoscale, 2013, 5, 6950–6959. [PubMed: 23787714]
11. Jashari F, Ibrahimi P, Johansson E, Ahlqvist J, Arnerlov C, Garoff M, Jaghagen EL, Wester P and Henein MY, Int J Mol Sci, 2015, 16, 19978–19988. [PubMed: 26307978]
12. Johnson RC, Leopold JA and Loscalzo J, Circ Res, 2006, 99, 1044–1059. [PubMed: 17095733]
13. Chin DD, Chowdhuri S and Chung EJ, Regenerative Engineering and Translational Medicine, 2019, 5, 74–85. [PubMed: 31106257]
14. Wang Y, Osborne MT, Tung B, Li M and Li Y, J Am Heart Assoc, 2018, 7.
15. Chung EJ, Cheng Y, Morshed R, Nord K, Han Y, Wegscheid ML, Auffinger B, Wainwright DA, Lesniak MS and Tirrell MV, Biomaterials, 2014, 35, 1249–1256. [PubMed: 24211079]

16. Chung EJ, Mlinar LB, Nord K, Sugimoto MJ, Wonder E, Alenghat FJ, Fang Y and Tirrell M, Adv Healthc Mater, 2015, 4, 367–376. [PubMed: 25156590]
17. Trent A, Marullo R, Lin B, Black M and Tirrell M, Soft Matter, 2011, 7, 9572–9582.
18. Yoo SP, Pineda F, Barrett JC, Poon C, Tirrell M and Chung EJ, ACS Omega, 2016, 1, 996–1003. [PubMed: 27917409]
19. Poon C, Sarkar M and Chung EJ, 2017, DOI: doi:10.3791/56625, e56625.
20. Li F, Li C, Liu X, Chen Y, Bai T, Wang L, Shi Z and Feng S, Chemistry, 2012, 18, 11641–11646. [PubMed: 22886785]
21. Cui H, Webber MJ and Stupp SI, Biopolymers, 2010, 94, 1–18. [PubMed: 20091874]
22. Chung EJ and Tirrell M, Adv Healthc Mater, 2015, 4, 2408–2422. [PubMed: 26085109]
23. Marc SKS, Roy D, Amis Eric J., Becker Matthew L., Advanced Materials, 2008, 20, 1830–1836.
24. Wang J, Poon C, Chin D, Milkowski S, Lu V, Hallows KR and Chung EJ, Nano Research, 2018, 11, 5584–5595.
25. Arleth L, Ashok B, Onyuksel H, Thiyagarajan P, Jacob J and Hjelm RP, Langmuir, 2005, 21, 3279–3290. [PubMed: 15807565]
26. Kastantin M, Ananthanarayanan B, Karmali P, Ruoslahti E and Tirrell M, Langmuir, 2009, 25, 7279–7286. [PubMed: 19358585]
27. Wada T, McKee MD, Steitz S and Giachelli CM, Circ Res, 1999, 84, 166–178. [PubMed: 9933248]
28. Trion A, Schutte-Bart C, Bax WH, Jukema JW and van der Laarse A, Mol Cell Biochem, 2008, 308, 25–33. [PubMed: 17909945]
29. Tang W, Ma Y, Xie S, Guo K, Katzenmeyer B, Wesdemiotis C and Becker ML, Biomacromolecules, 2013, 14, 3304–3313. [PubMed: 23931528]
30. Lee JS and Tung CH, Chembiochem, 2011, 12, 1669–1673. [PubMed: 21661088]
31. Chung EJ, Chien KB, Aguado BA and Shah RN, Tissue Eng Part A, 2013, 19, 2664–2673. [PubMed: 23790163]
32. Drake MT, Clarke BL and Khosla S, Mayo Clin Proc, 2008, 83, 1032–1045. [PubMed: 18775204]
33. Aikawa E, Nahrendorf M, Sosnovik D, Lok VM, Jaffer FA, Aikawa M and Weissleder R, Circulation, 2007, 115, 377–386. [PubMed: 17224478]
34. Aikawa E, Nahrendorf M, Figueiredo JL, Swirski FK, Shtatland T, Kohler RH, Jaffer FA, Aikawa M and Weissleder R, Circulation, 2007, 116, 2841–2850. [PubMed: 18040026]
35. Celeng C, de Keizer B, Merkely B, de Jong P, Leiner T and Takx RAP, Curr Cardiol Rep, 2018, 20, 11. [PubMed: 29435774]
36. Gustafson HH, Holt-Casper D, Grainger DW and Ghandehari H, Nano Today, 2015, 10, 487–510. [PubMed: 26640510]
37. Arvizo RR, Miranda OR, Moyano DF, Walden CA, Giri K, Bhattacharya R, Robertson JD, Rotello VM, Reid JM and Mukherjee P, PloS one, 2011, 6, e24374–e24374. [PubMed: 21931696]
38. Weiger MC, Park JJ, Roy MD, Stafford CM, Karim A and Becker ML, Biomaterials, 2010, 31, 2955–2963. [PubMed: 20106520]
39. Murphy MB, Hartgerink JD, Goepferich A and Mikos AG, Biomacromolecules, 2007, 8, 2237–2243. [PubMed: 17530891]
40. Low SA and Kopecek J, Adv Drug Deliv Rev, 2012, 64, 1189–1204. [PubMed: 22316530]
41. Maldonado N, Kelly-Arnold A, Vengrenyuk Y, Laudier D, Fallon JT, Virmani R, Cardoso L and Weinbaum S, Am J Physiol Heart Circ Physiol, 2012, 303, H619–628. [PubMed: 22777419]
42. Poon C, Chowdhuri S, Kuo C-H, Fang Y, Alenghat FJ, Hyatt D, Kani K, Gross ME and Chung EJ, ACS Biomaterials Science & Engineering, 2017, DOI: 10.1021/acsbiomaterials.7b00600.
43. Chung EJ, Mlinar LB, Sugimoto MJ, Nord K, Roman BB and Tirrell M, Nanomedicine, 2015, 11, 479–487. [PubMed: 25194999]
44. Nicholls SJ, Tuzcu EM, Wolski K, Sipahi I, Schoenhagen P, Crowe T, Kapadia SR, Hazen SL and Nissen SE, J Am Coll Cardiol, 2007, 49, 263–270. [PubMed: 17222740]

45. Reynolds JL, Joannides AJ, Skepper JN, McNair R, Schurgers LJ, Proudfoot D, Jahnen-Dechent W, Weissberg PL and Shanahan CM, J Am Soc Nephrol, 2004, 15, 2857–2867. [PubMed: 15504939]

46. Shioi A, Nishizawa Y, Jono S, Koyama H, Hosoi M and Morii H, Arterioscler Thromb Vasc Biol, 1995, 15, 2003–2009. [PubMed: 7583582]

47. Abedin M, Tintut Y and Demer LL, Arterioscler Thromb Vasc Biol, 2004, 24, 1161–1170. [PubMed: 15155384]

48. Rattazzi M, Bennett BJ, Bea F, Kirk EA, Ricks JL, Speer M, Schwartz SM, Giachelli CM and Rosenfeld ME, Arterioscler Thromb Vasc Biol, 2005, 25, 1420–1425. [PubMed: 15845913]

49. Meng F, Wang J, Ping Q and Yeo Y, ACS Nano, 2018, 12, 6458–6468. [PubMed: 29920064]

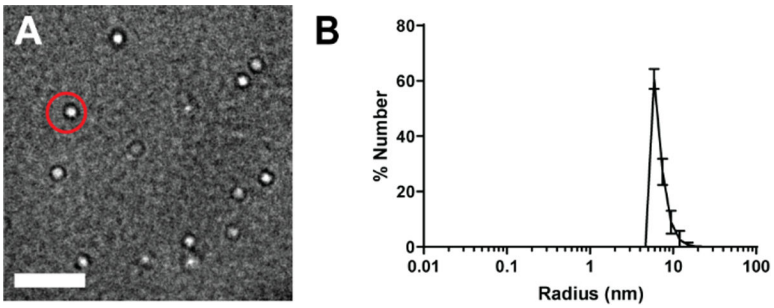

Fig. 1.

Characterization of HA PAMs. A) TEM images show HA PAMs (red circle) are spherical and monodisperse. Scale bar 100 nm. B) DLS measurements show HA PAMs to have a radius of approximately 8.0 ± 1.5 nm (N≥3).

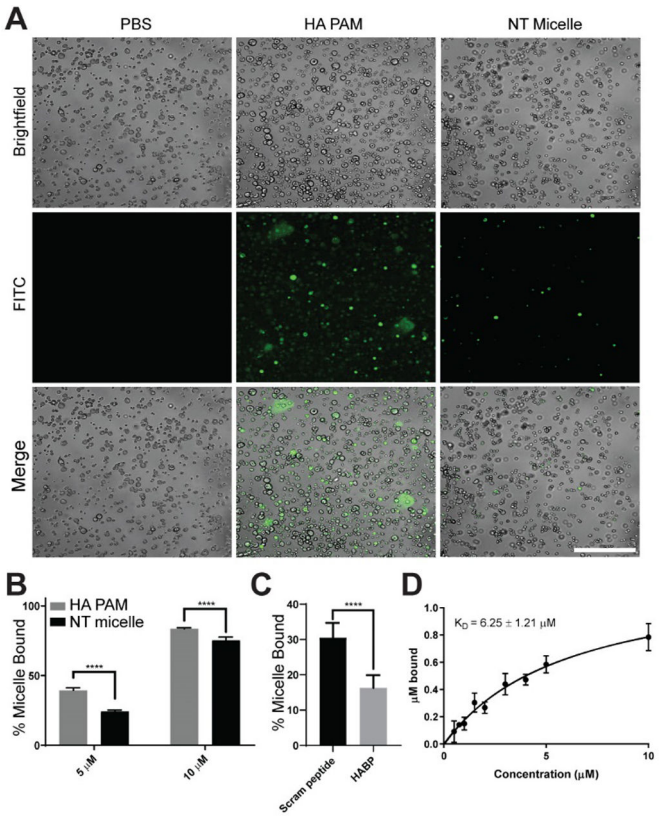

Fig. 2.

Micelle binding to HA microcrystals. A) Confocal images show HA PAMs (green, 5 μM) bind to HA microcrystals (brightfield) to a greater extent than NT micelles which exhibited minimal binding. Scale bar 100 μm. B) Quantification of micelle binding to HA microcrystals at 5 and 10 μM. **** indicates p≤0.0001. C) Competition assay shows specificity of HABP binding to HA. HA PAM bound 1.8-fold greater to HA microcrystals preincubated with scrambled HABPs (30.5 ± 4.2%) vs. HABPs (16.3 ± 3.6%, **** p≤0.0001, N=6) D) Binding isotherm of HA PAM on HA microcrystals show a K_D of 6.25 ± 1.21 μM (N=3).

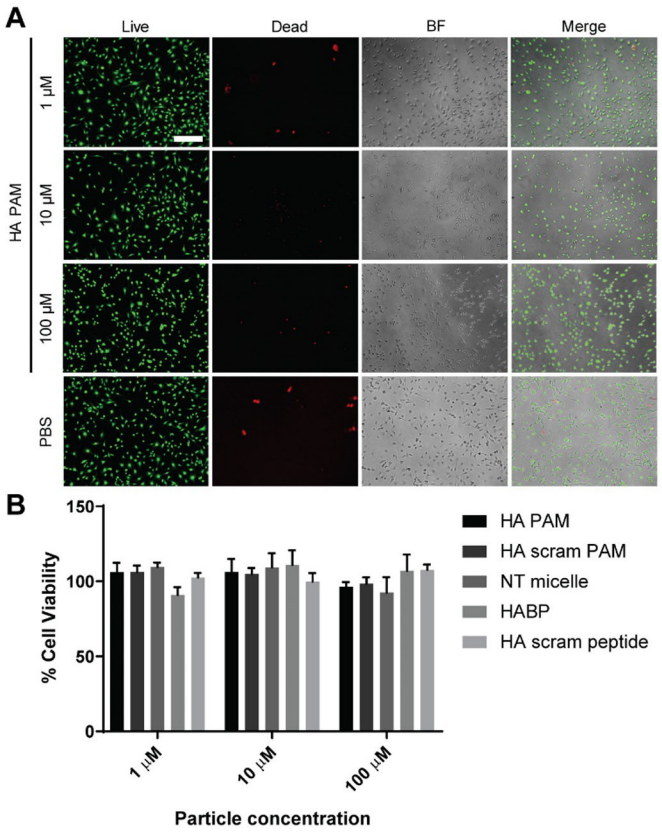

Fig. 3.

In vitro biocompatibility of micelles. A) MOVAS cells treated with HA PAMs for 48 hours show cell viability is similar to PBS-treated controls via Live/Dead assay (N=6). Scale bar 100 μm. B) MTS assay on MOVAS cells treated with HA PAMs, HA scram PAMs, NT micelles, HABPs, or HA scram peptides (1, 10, 100 μM) show little to no toxicity on cells after 48 hours of treatment (N=6).

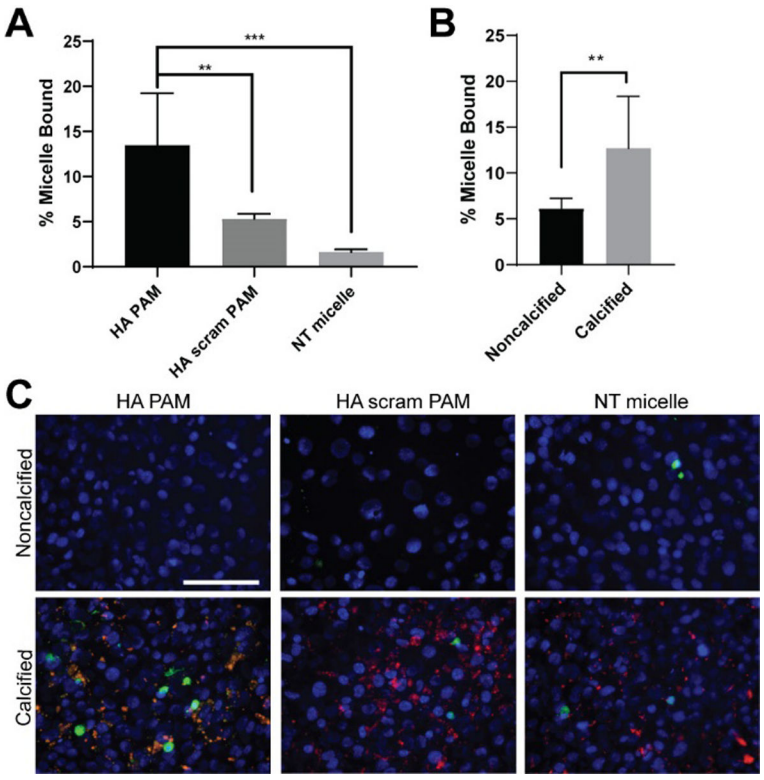

Fig. 4.

Micelle binding on calcified MOVAS cells. A) HA PAM, HA scram PAM, and NT micelle binding on MOVAS cells cultured for 21 days in osteogenic media. HA PAMs have a 2.5-fold increase in binding when compared to HA scram PAMs and an 8-fold increase in binding compared to NT micelle (N=8). ** $p \leq 0.01$, *** $p \leq 0.001$. B) HA PAMs bind to calcified MOVAS cells cultured in osteogenic media to a greater extent than nonosteogenic MOVAS cells cultured in growth media for 21 days (calcified: 12.7 ± 5.7% vs noncalcified: 6.1 ± 1.1%, N=8). **$p \leq 0.01$. C) Fluorescence images demonstrate HA PAMs colocalized to calcifications on MOVAS cells (DAPI, blue; ARS, red; micelles, green). Scale bar 100 μm.

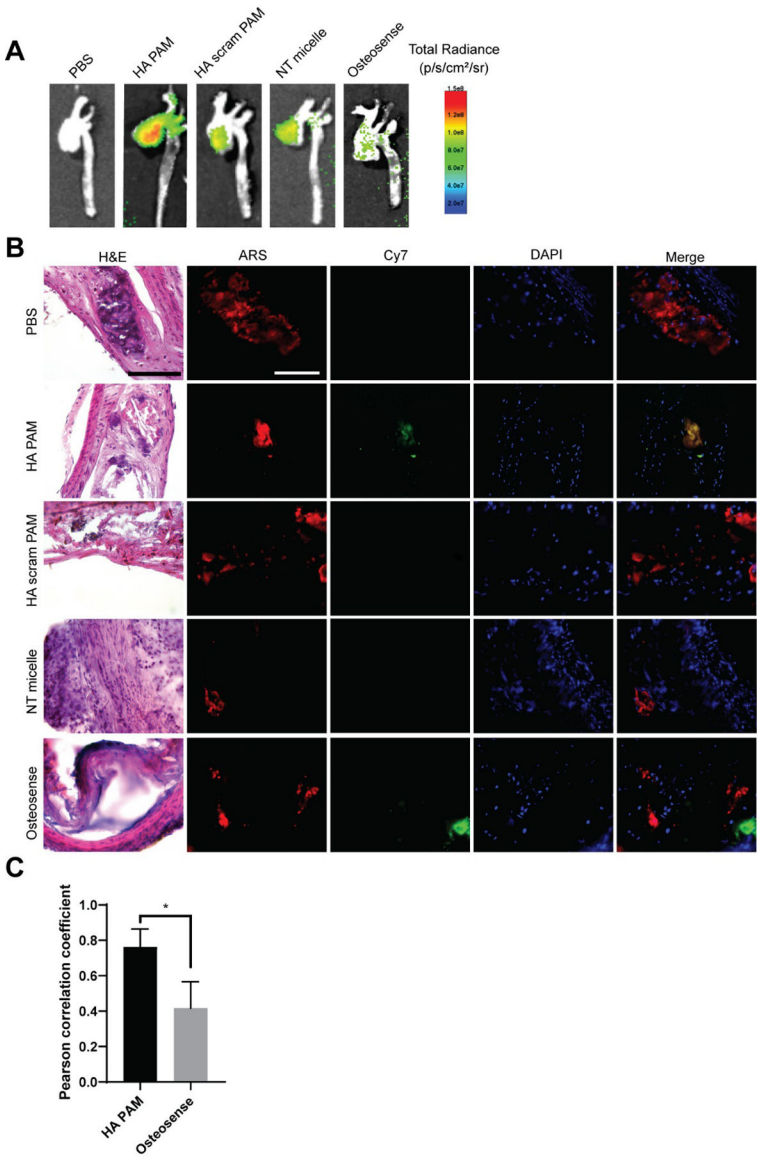

Fig. 5.

Aortas of ApoE −/− mice 24 hours post-administration of HA PAMs, HA scram PAMs, NT micelles (N=4), Osteosense, or PBS (N=3). A) *Ex vivo* NIR fluorescence demonstrate enhanced accumulation of HA PAMs compared to other groups. B) Brachiocephalic artery sections stained with H&E show plaque morphology (arrows: calcification). Artery sections were also stained with ARS (red) for calcification and DAPI (blue) for nuclei. Mice treated with HA PAM (green) show colocalization with calcifications (yellow in merged image). No signal is apparent for PBS-, NT micelle-, and HA scram PAM-treated aortas. Osteosense also showed some fluorescence signal in areas of calcification. Scale bar 100 μm. C) Quantification of colocalization of HA PAM or Osteosense with ARS show strong HA PAM colocalization (0.76 ± 0.1) with ARS compared to Osteosense (0.42 ± 0.15). *p≤0.05.

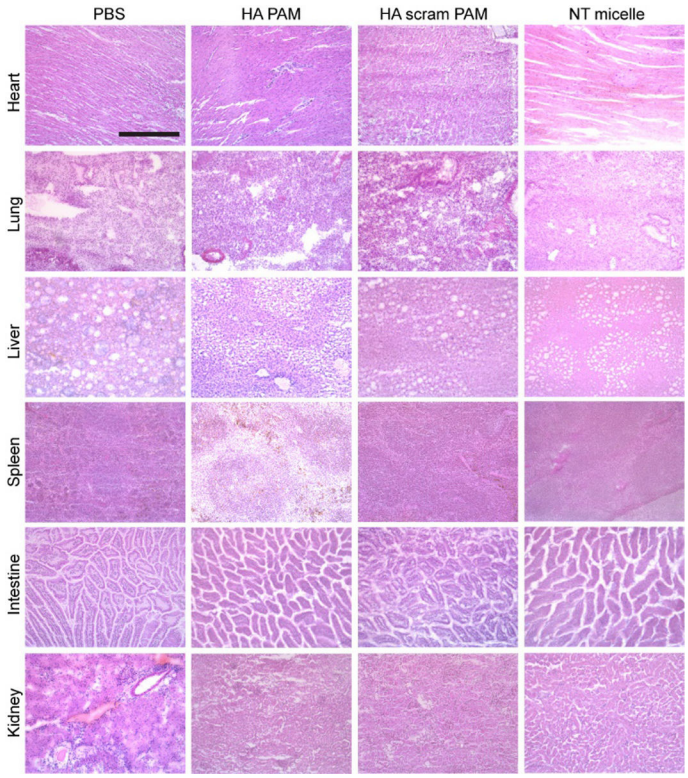

Fig. 6.

Representative H&E staining of organs after micelle administration. Micelle-treated mice exhibit no toxicity based on morphology of sectioned tissue when compared with PBS-treated control. Scale bar 100 μm.

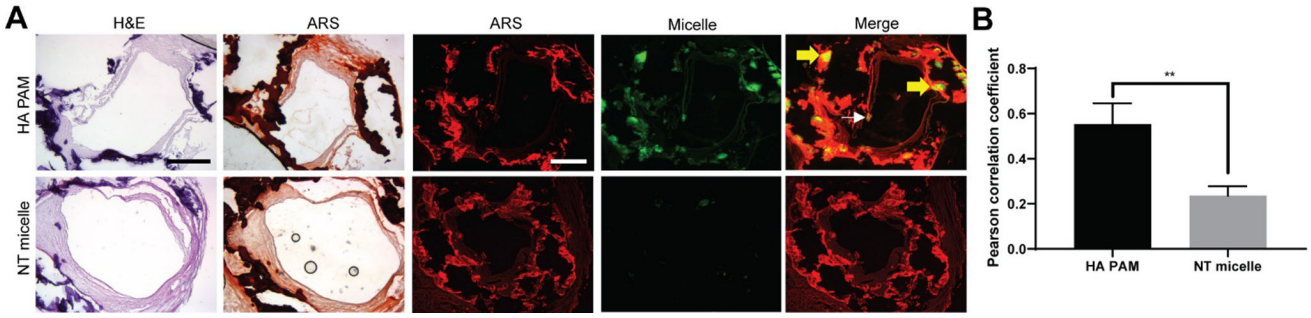

Fig. 7.

Micelle binding on discarded human tibial artery tissues with severe arterial calcification. Arteries incubated with HA PAMs or NT micelles were embedded, sectioned and stained with A) H&E and ARS (N=3). HA PAMs show strong signal and penetration through bulk calcification, while NT micelles have minimal signal. Scale bars 500 μm. B) HA PAMs exhibit strong colocalization (0.55 ± 0.09) with calcifications comapred to NTmicelles (0.24 ± 0.04). ** $p \leq 0.01$.

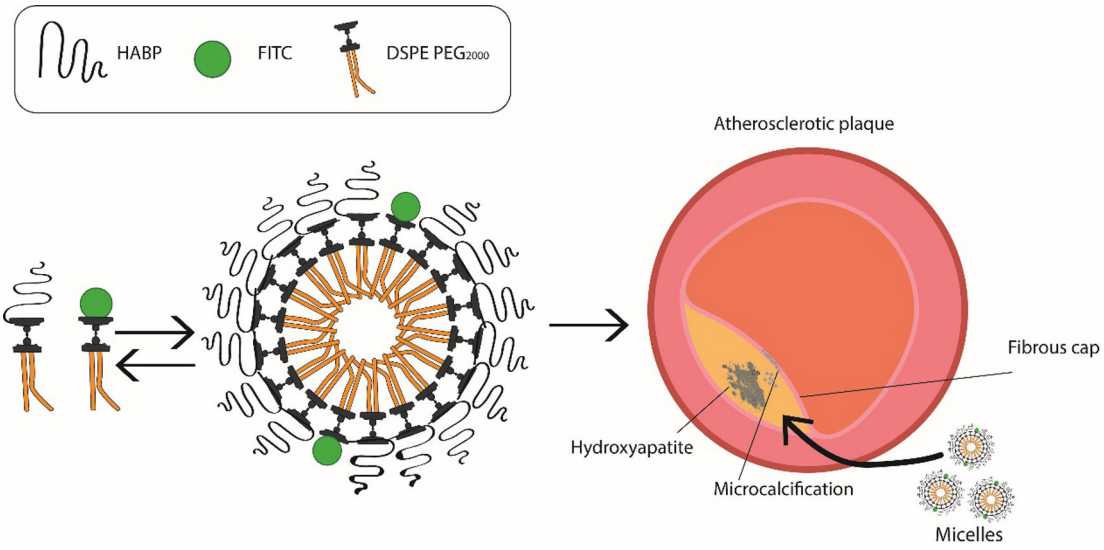

Scheme 1.

Schematic of HA PAM synthesis and targeting calcification found in atherosclerotic plaque.

Table. 1

Size and zeta potential measurements of micelles.

Particle	Radius (nm)	PDI	Zeta Potential (mV)
HA PAM	8.0 ± 1.5	0.30 ± 0.04	−2.7 ± 2.2
NT micelle	6.6 ± 0.3	0.13 ± 0.02	−0.9 ± 1.1